


Article

Hydrogenation Thermodynamics of $\text{Ti}_{16}\text{V}_{60}\text{Cr}_{24-x}\text{Fe}_x$ Alloys ($x = 0, 4, 8, 12, 16, 20, 24$)

Francia Ravalison and Jacques Huot * 

Hydrogen Research Institute, Université du Québec à Trois-Rivières, Trois-Rivières, QC G9A5H7, Canada; francia.ravalison.soloarivelo@uqtr.ca

* Correspondence: jacques.huot@uqtr.ca; Tel.: +1-819-376-5011 (ext. 3576); Fax: +1-819-376-5164

Abstract: The effect of the partial substitution of Cr with Fe on the thermodynamic parameters of vanadium-rich $\text{Ti}_{16}\text{V}_{60}\text{Cr}_{24-x}\text{Fe}_x$ alloys ($x = 0, 4, 8, 12, 16, 20, 24$) was investigated. For each composition, a pressure–concentration isotherm (PCI) was registered at 298, 308, and 323 K. The PCI curves revealed a reduction in plateau pressure and a decrease in desorbed hydrogen capacity with an increasing amount of Fe. For all alloys, about 50% or less of the initial hydrogen capacity was desorbed for all chosen temperatures. Entropy (ΔS) and enthalpy (ΔH) values were deduced from corresponding Van't Hoff plots of the PCI curves: the entropy values ranged from -150 to -57 J/K·mol H_2 , while the enthalpy values ranged from -44 to -21 kJ/mol H_2 . They both decreased with an increasing amount of Fe. Plotting ΔS as function of ΔH showed a linear variation that seems to indicate an enthalpy–entropy compensation. Moreover, a quality factor analysis demonstrated that the present relationship between entropy and enthalpy is not of a statistical origin at the 99% confidence level.

Keywords: hydrogen storage; vanadium-rich alloy; BCC alloys; thermodynamics; pressure composition isotherm enthalpy; entropy; EEC compensation



Citation: Ravalison, F.; Huot, J. Hydrogenation Thermodynamics of $\text{Ti}_{16}\text{V}_{60}\text{Cr}_{24-x}\text{Fe}_x$ Alloys ($x = 0, 4, 8, 12, 16, 20, 24$). *Hydrogen* **2024**, *5*, 29–38. <https://doi.org/10.3390/hydrogen5010003>

Academic Editor: Jin-Yoo Suh

Received: 10 November 2023

Revised: 13 December 2023

Accepted: 25 January 2024

Published: 26 January 2024



Copyright: © 2024 by the authors. Licensee MDPI, Basel, Switzerland. This article is an open access article distributed under the terms and conditions of the Creative Commons Attribution (CC BY) license (<https://creativecommons.org/licenses/by/4.0/>).

1. Introduction

For the full implementation of hydrogen as an energy vector, safe and low-cost means of storing hydrogen should be available. Many ways to store hydrogen are available such as high-pressure, cryogenic liquid hydrogen, porous materials, liquid hydrogen carriers (e.g., ammonia), complex metal hydrides and intermetallic hydrides [1]. Metal hydrides are promising candidates for many stationary and mobile hydrogen storage applications. Because of their high volumetric densities and relatively low pressures of operation under mild temperatures, metal hydrides are ideally suited for a broad range of applications [2].

There are many families of hydride-forming intermetallic compounds. Usually, they are formed by a combination of elements that have a high affinity for hydrogen (A) and elements with a low affinity for hydrogen (B). The most usual A/B combinations are AB_5 (e.g., LaNi_5), AB_2 (ZrV_2), AB_3 (CeNi_3), A_2B_7 (Y_2Ni_7), AB (TiFe) and A_2B (Mg_2Ni) [3]. These families have been extensively studied using different combinations of A and B elements, the partial substitution of an A (or B) element by another A (or B) element, the addition of a catalyst, mechanical deformation, etc.

Another interesting family of metal hydrides is the solid solution Body-Centered Cubic (BCC) alloys. These alloys are frequently based on vanadium, and they have attracted attention due to their high maximum hydrogen capacity (~ 4 wt.%) [1–8]. The process of the hydrogenation of pure vanadium occurs two steps. In the first step, the monohydride VH is formed at a very low hydrogen pressure (< 1 Pa), while the formation of the dihydride VH_2 occurs at much higher pressure (0.4 MPa at 313 K) [4]. The monohydride is so stable that it can only be desorbed at a very high temperature (750 K). The high stability of the monohydride means that the effective capacity of vanadium hydride is about 2 wt.%. The

thermodynamics of hydrogenation could be changed by alloying vanadium with other elements to create binary, ternary or quaternary alloys. This modification of thermodynamics is due to the change in the electronic density of state, ionicity and the lattice's expansion [4]. As Ti forms a solid solution with V for a large range of compositions, it was the first binary system to be investigated for the formation of hydrides [5]. It was found that alloying V with Ti increases the stability of the hydride (with a lower plateau pressure), while alloying Cr with V leads to a less stable dihydride [6,7]. As we will see below, by choosing the right proportion of elements, a ternary alloy could have attractive hydrogen storage characteristics.

However, to meet the commercial needs for hydrogen storage, two aspects should be taken into consideration. The first one is the first hydrogenation, the so-called activation. For vanadium-based metal hydrides, activation is usually slow, requiring a high temperature and/or pressure [9]. Previous studies have solved these drawbacks by using additives [10–13] or mechanical processing [14–19]. The second aspect is thermodynamics. To be commercially attractive, the alloy should have a plateau pressure of a few bars near room temperature. By alloying vanadium with other metals, the plateau pressure and reversibility could be improved [18].

As mentioned previously, the hydrogenation of BCC metal hydrides usually occurs in two stages. First, the phase transition of a BCC solid solution (α -phase) to an intermediate Body-Centered Tetragonal (BCT) monohydride (β -phase) that is associated with a low plateau pressure occurs. Second, the formation of a Face-Centered Cubic (FCC) phase (γ -phase) that is related to a higher plateau pressure with a ratio of hydrogen atoms over metallic atoms (H/M) of approximately two ($H/M \approx 2$) occurs [19]. The hydrogen absorption and desorption reactions can occur at moderate temperatures and pressures since the γ -phase is usually not very stable. Consequently, the reversible hydrogen capacity is reduced by approximately half in vanadium metal, which is not sufficient for practical applications [20]. This issue has been partially resolved by adding alloying elements [21–29]. For example, Aoki et al. have reported that in the system $Ti_{12}Cr_{23}V_{65}$, when V is substituted with Fe, the cyclability is improved: $Ti_{12}Cr_{23}V_{64}Fe_1$ released 97% of its initial capacity, while the Fe-free alloy only desorbed 88% [30]. Towata et al. studied the effect of partial niobium and iron substitution on the short-term cycle durability of hydrogen storage Ti-V-Cr alloys [31]. Partial iron substitution enhanced the cyclability of the $Ti_{16}V_{50}Cr_{34}$ alloy but reduced its hydrogen storage capacity. Partial niobium substitution was not only favorable for the $Ti_{25}Cr_{50}V_{25}$ alloy's cyclability; it also did not affect the hydrogen capacity [31]. Moreover, the study of Zr substitution for Ti on the hydrogen absorption–desorption characteristics of $Ti_{1-x}Zr_xCrV$ ($x = 0, 0.05, 0.1$ and 0.1) revealed that the presence of a small amount of Zr has advantageous effects on the hydrogen absorption properties of Ti-Cr-V as it suppresses TiH_2 phase separation and decreases hysteresis [32].

The hydrogenation/dehydrogenation enthalpy and entropy are obtained from Van't Hoff plots that are generated from a series of PCI (pressure–composition isotherm) measurements at different temperatures [33]. The enthalpy (ΔH) and the entropy (ΔS) of the metal hydride formation are calculated from the equation $\ln(p_{eq}/p_0) = (\Delta H/RT) - (\Delta S/R)$, where R is the gas constant. In general, the entropy change ΔS is mainly due to the hydrogen gas. It is approximately -130 J/mol·K and is considered invariant and independent of the nature of the metal hydride. The enthalpy should be of the order of -30 kJ/mol H_2 to desorb hydrogen under normal temperature and pressure conditions [34]. However, it was found that enthalpies and entropies derived from Van't Hoff or Arrhenius plots exhibit strong linear correlations in many thermodynamic or kinetic experiments for a series of similar reactions [35–38]. This so-called enthalpy–entropy compensation (EEC) has been the subject of investigations [39–42]. Griessen and Dam have reported an accurate verification scheme that allows one to determine the nature of EEC using the so-called K-CQF method [43]. This method permits one to distinguish if the EEC measured is a true effect or just an artefact due to the limited number and range of data points.

In this paper, the effect of Fe substitution on the thermodynamic properties of $\text{Ti}_{16}\text{V}_{60}\text{Cr}_{24-x}\text{Fe}_x$ alloys for $x = 0, 4, 8, 12, 16, 20, 24$ is reported. Firstly, PCI curves of all alloys will be compared. Then, enthalpies and entropies will be deduced from Van't Hoff plots. Finally, since we have a series of measurements with a systematic change in composition, we will address the correlation between enthalpy and entropy for this composition system.

2. Materials and Methods

All alloys were synthesized by arc melting under argon to avoid any oxidation. The elements were purchased from Alfa-Aesar (Tewksbury, MA, USA) with the following purities: Ti (99.95%), V (99%), Cr (99%), Zr (99.95) and Fe (99.9%). They alloys were re-melted several times to ensure homogeneity. Then, they were hand-crushed in an argon-filled glove box. Hydrogenation measurements were carried out with a homemade Sievert-type apparatus. Each sample was first fully hydrogenated at room temperature under 3 MPa of hydrogen. Then, it was kept under pressure while the temperature was raised to the desired PCI temperature. Only desorption PCIs were recorded. The PCI measurements were performed at 298, 308 and 323 K.

3. Results and Discussion

3.1. Microstructure, Crystal Structure and First Hydrogenation

The microstructure, crystal structure and first hydrogenation were reported in our previous paper [44]. It was found that the microstructure consisted of two main phases: a matrix with a chemical composition close to the nominal one and a Zr-rich region. The crystal structure of the main phases of all as-cast alloys was BCC. For $x \geq 12$, the BCC phase abundance decreased, and a C14 Laves phase appeared. The lattice parameter of the BCC phase decreased linearly with an increasing Fe proportion. After hydrogenation, the BCC phase was converted into a BCT phase for all hydrides, and a C14 phase appeared for $x = 4$ and 8. For $x \geq 16$, a C15 phase was present. Table 1 shows the hydrogen capacity and the crystal structure in the as-cast and hydrogenated states of all investigated alloys.

Table 1. Maximum hydrogen capacity upon activation and crystal structure of hydrides [44].

x	Maximum Hydrogen Capacity (wt.%)	Crystal Structure	
		As-Cast	After Hydrogenation
0	3.78	BCC (100%)	BCT (100%)
4	3.09	BCC (100%)	BCT (80%) + C14 (20%)
8	2.08	BCC (100%)	BCT (78%) + C14 (22%)
12	1.89	BCC (79%) + C14 (21%)	BCT (76%) + C14 (24%)
16	2.06	BCC (77%) + C14 (23%)	BCT (58%) + C14 (24%) + C15 (18%)
20	1.94	BCC (74%) + C14 (26%)	BCT (64%) + C14 (23%) + C15 (13%)
24	1.99	BCC (72%) + C14 (28%)	BCT (53%) + C14 (37%) + C15 (11%)

3.2. Pressure Composition Isotherms (PCIs)

Figure 1 shows the desorption PCI curves of all alloys at temperatures of 298, 308 and 323 K. All isotherms show incomplete desorption and a sloping plateau pressure. This is a common behaviour of BCC alloys that indicates that these alloys desorb hydrogen in two steps: at high pressures, a dihydride-to-monohydride transformation occurs, and at low pressures, a monohydride dehydrogenation occurs [18,45]. In our case, as the lowest measurable pressure was 10 kPa, we could only register the dihydride-to-monohydride transformation.

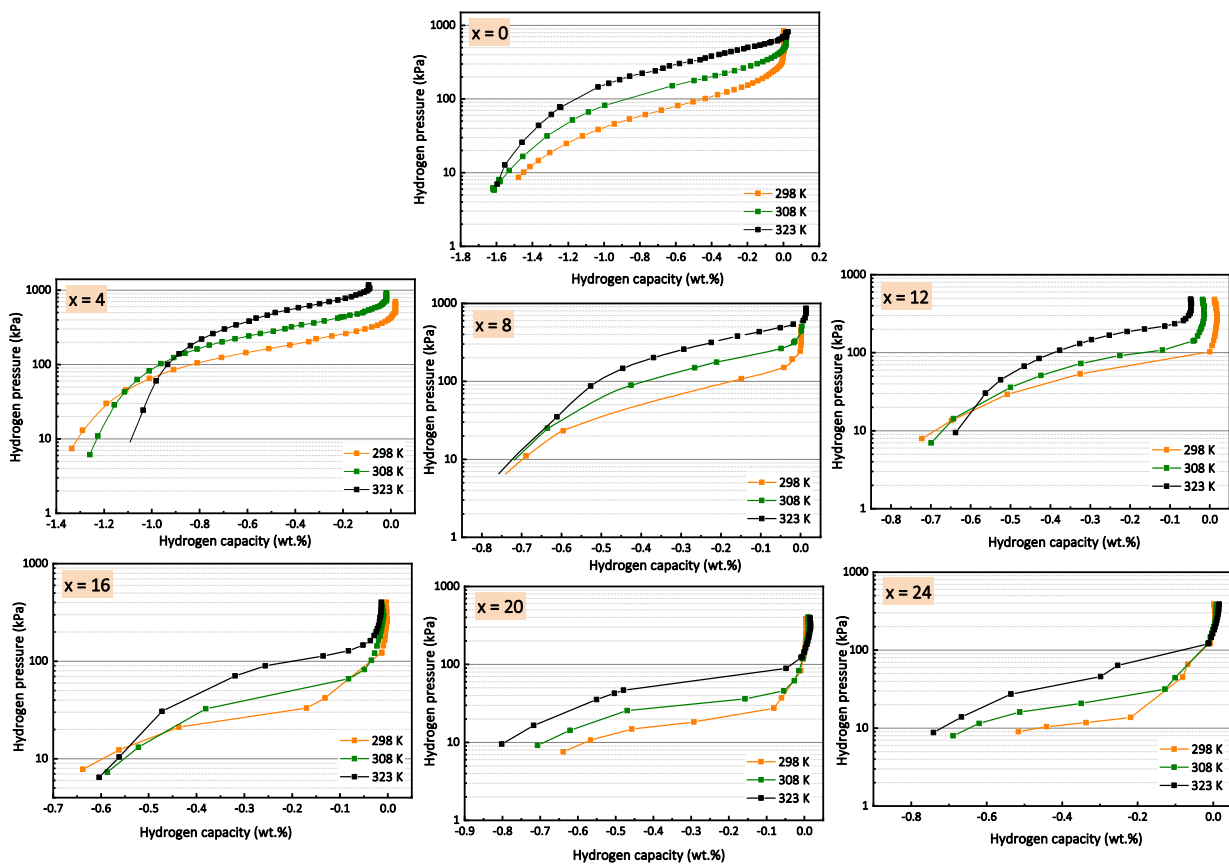


Figure 1. PCI desorption curves of $\text{Ti}_{16}\text{V}_{60}\text{Cr}_{24-x}\text{Fe}_x$ alloy for $x = 0, 4, 8, 12, 16, 20, 24$, at 298, 308 and 323 K.

As only the desorption isotherm was registered and the capacity is lowered at higher temperatures due to a low critical point, the isotherms were centered on their inflection points (i.e., middle of the plateau). It is also at this point that the equilibrium pressure was taken for the Van't Hoff plots.

3.3. Enthalpy and Entropy

The Van't Hoff plots constructed from the PCI curves of each alloy are presented in Figure 2.

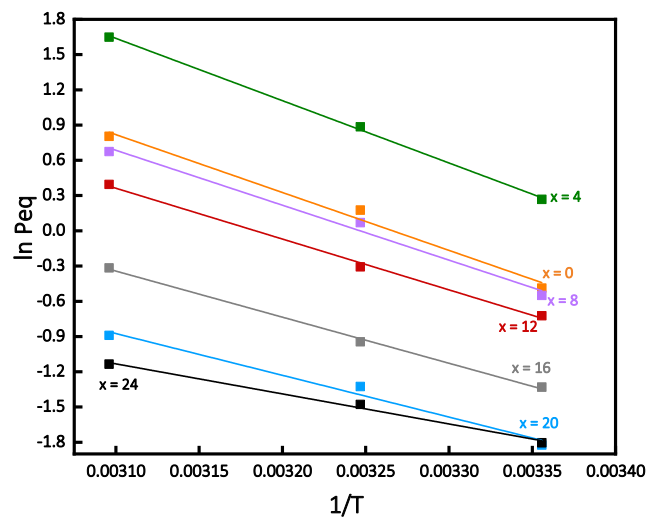


Figure 2. Van't Hoff curves of $\text{Ti}_{16}\text{V}_{60}\text{Cr}_{24-x}\text{Fe}_x$ alloy for $x = 0, 4, 8, 12, 16, 20, 24$, at 298, 308 and 323 K.

For each composition, the entropy (ΔS) and enthalpy (ΔH), were calculated from the intercept and slope. The results are given in Table 2. As a comparison, the enthalpy and the entropy of the formation of pure vanadium hydride are -40 kJ/mol H_2 and -140 J/K·mol H_2 , respectively [7]. Here, we can notice that from $x = 0$ to 8, the enthalpies and entropies are in the same ranges as those of the pure vanadium hydride.

Table 2. Entropy and enthalpy values of the formation of all hydrides.

x	ΔS (J/K·mol H_2)	ΔH (kJ/mol H_2)
0	-134 ± 14	-41 ± 5
4	-150 ± 12	-44 ± 4
8	-126 ± 12	-39 ± 4
12	-114 ± 6	-36 ± 2
16	-98 ± 5	-33 ± 2
20	-84 ± 12	-30 ± 4
24	-57 ± 5	-21 ± 2

Figure 3 displays variations in ΔS and ΔH as functions of the Fe content. We found a linear decrease in both enthalpy and entropy with an increasing iron content. Lynch et al. have reported the same trend [46]. They found that for the system $(V_{0.9}Ti_{0.1})_{1-x}Fe_x$ ($x = 0, 0.01, 0.02, 0.05, 0.075$), the enthalpy went from (-51.79 ± 0.36) to (-40.00 ± 2.70) kJ/mol H_2 , and the entropy changed from (-149.4 ± 1.0) to (-136.0 ± 8.1) J/K·mol H_2 . They attributed the reduction in enthalpy to a decrease in the binding energy of hydrogen to the metal. Moreover, the lattice parameter was also diminishing, causing a shrinkage of the size of the tetrahedral site occupied by hydrogen. Both effects were suspected to destabilize the dihydride and then qualitatively reduce the desorption enthalpy. They explained the drop in entropy by an increase in the vibrational entropy of the hydrogen in the hydride lattice. As mentioned earlier, the enthalpy can largely vary but, usually, the entropy value is around -130 J/K·mol H_2 . Here, there is a clear dependence of entropy on the composition.

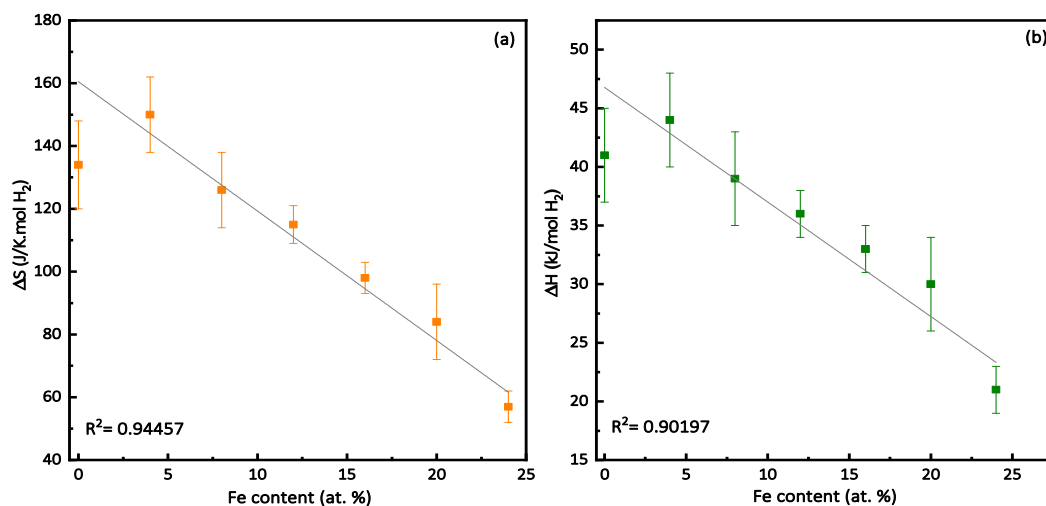


Figure 3. Variations in (a) ΔS and (b) ΔH with Fe content.

3.4. Enthalpy–Entropy Compensation

Figure 4 presents the variation in entropy (ΔS) as a function of enthalpy (ΔH) for the $Ti_{16}V_{60}Cr_{24-x}Fe_x$ alloy for $x = 0, 4, 8, 12, 16, 20, 24$. It shows a linear variation that seems to be a case of enthalpy–entropy compensation (EEC).

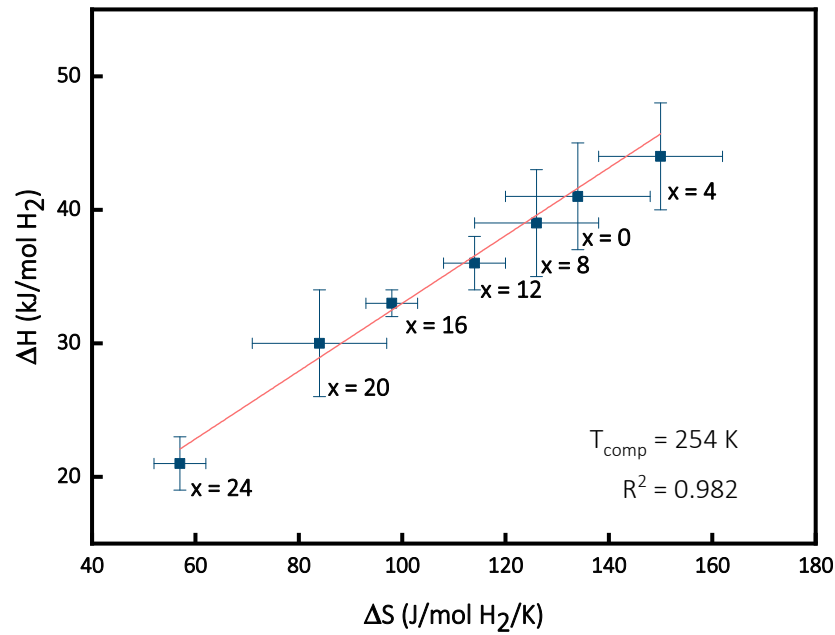


Figure 4. Variation in enthalpy (ΔH) as a function of entropy (ΔS) for $\text{Ti}_{16}\text{V}_{60}\text{Cr}_{24-x}\text{Fe}_x$ alloy for $x = 4, 8, 12, 16, 20, 24$.

As mentioned above, Griessen and Dam introduced a method called combined K-CQF to verify the nature of EEC. The parameter CQF is a dimensionless factor that is a compensation quality factor, while K is a parameter that indicates the position of the coalescence [43]. The steps for determining K and CQF are as follows:

Step 1

The first step consists of calculating the harmonic mean temperature T_{hm} using the following equation:

$$T_{hm} = \left(\frac{1}{M} \sum_{j=1}^M \frac{1}{T_j} \right)^{-1} \quad (1)$$

T_j with $j = 1, \dots, M$ is the temperature of the j -th measurement at which the equilibrium pressures of the N samples are determined [43]. In our case, $T_{low} = 298$ K and $T_{high} = 323$ K. Since we used three temperatures for measuring PCTs, $M = 3$, and we obtain $T_{hm} = 309$ K.

Step 2

The second step is to determine the temperature of compensation T_{comp} and the correlation coefficient R^2 . T_{comp} is the slope of the linear fit derived from the ΔH_i versus ΔS_i plot. The variation in the T_{comp} predictable from the change in the thermodynamic parameters is given by the R^2 value. An R^2 value of 1 means that T_{comp} is totally determined by the thermodynamic parameters. From Figure 4, we have $T_{comp} = 254$ K and $R^2 = 0.982$.

Step 3

The third step is finding T_{min} and calculating the coefficient K. There are two ways to determine T_{min} . Firstly, the following equation can be used:

$$T_{min} = \frac{T_{comp}}{R_{square}} \quad (2)$$

From Equation (2), the value of T_{min} is 258 K. Secondly, a graphical method may be used by extrapolating the Van't Hoff plots. Then, the temperature where the spread of the Van't Hoff curves is at a minimum is the T_{min} . Figure 5 presents this extrapolation for the Van't Hoff plots of Figure 2. The value of T_{min} in this case is 242 K.

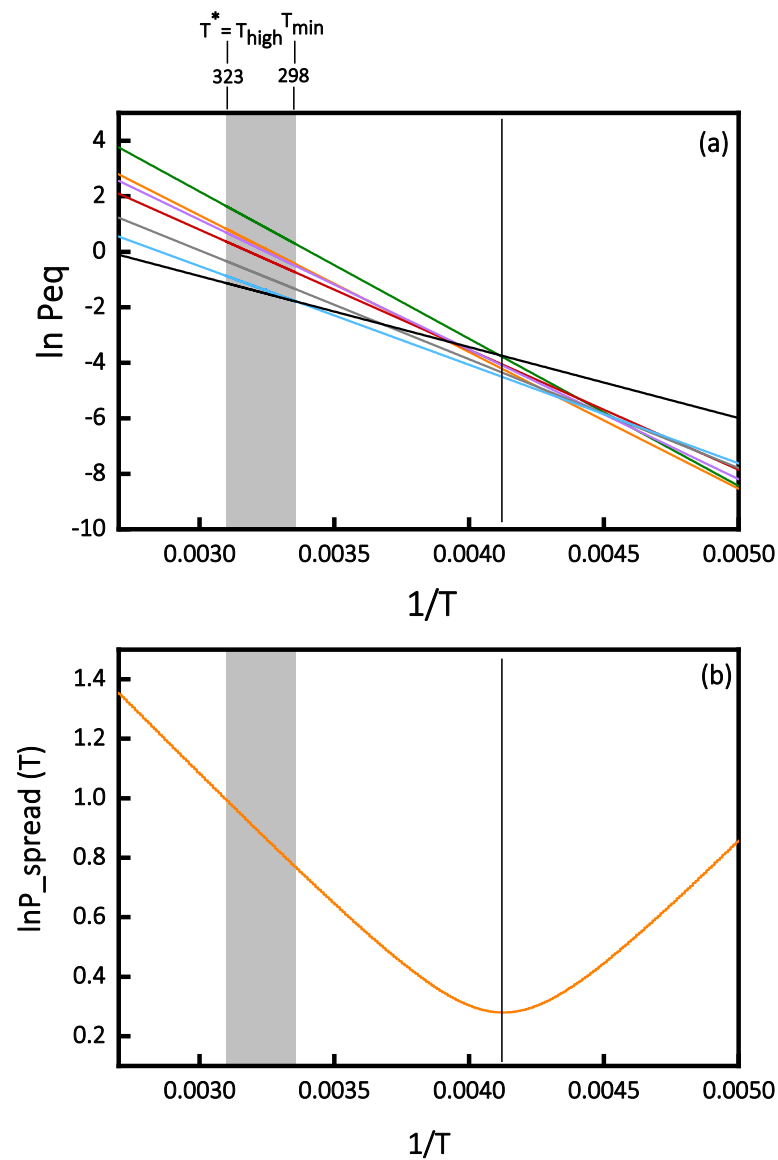


Figure 5. (a) Extrapolation of Van't Hoff plots. (b) Inverse temperature variation in the $\ln P_{spread}$ of the Van't Hoff plots in (a).

The coefficient K can be calculated using the following equation:

$$K = \frac{\frac{1}{T_{hm}} - \frac{1}{T_{min}}}{\frac{1}{2} \left(\frac{1}{T_{low}} - \frac{1}{T_{high}} \right)} \quad (3)$$

Step 4

The fourth step consists of calculating the CQF parameter. It is given by the following equation:

$$CQF = 1 - \sqrt{\frac{1 - R_{square}}{\left(\frac{1}{R_{square}}\right) \left(\frac{T_{comp}}{T^*}\right)^2 - 2 \left(\frac{T_{comp}}{T^*}\right) + 1}} \quad (4)$$

T^* is the temperature at which the measured $\ln P_{spread}$ is the largest. $T^* = T_{low}$ if $1/T_{min}$ is closer to $1/T_{high}$ or $T^* = T_{high}$ if $1/T_{min}$ is closer to $1/T_{low}$. In our case, as $1/T_{min}$ is closer to $1/T_{low}$, consequently, $T^* = T_{high} = 323$ K.

All useful parameters to determine K and CQF are summarized in Table 3. As specified, T_{min} can be either calculated from Equation (2) or deduced from the $\ln P_{spread}$ versus $1/T$ plot. As K is dependent on T_{min} , we obtained two different values of K. After completing all calculations, we obtained values of $K = -6.909$ (for $T_{min} = 242$ K), $K = -4.902$ (for $T_{min} = 258$ K) and $CQF = 0.44219$.

Table 3. Useful parameters for determining K and CQF according to [43].

T_{hm} (K)	T_{comp} (K)	R^2	T_{min} (K) (from Equation (2))	T_{min} (K) (from Figure 5)	T^* (K)
309	254	0.982	258	242	323

To draw a conclusion, Griessen and Dam proposed a graphical method (Figure 6), a 95% or 99% confidence level (CL) contour that depends only on the number of samples. If the (K, CQF) point lays outside the CL% contour, then the EEC is not of a statistical origin at this confidence level [43].

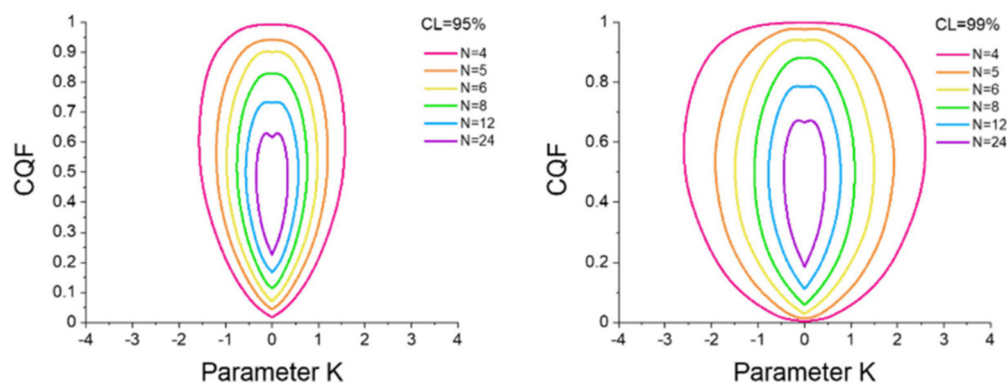


Figure 6. Confidence contours of 95% (left panel) and 99% (right panel) for $N = 4$ up to $N = 15$. From Ref. [43] with permission.

If we refer to Figure 6, for both values of K, the values of the pair (K, CQF) lie outside the 99% confidence contour. Thus, even though CQF is lower than 0.9, the EEC is not due to a statistical effect.

4. Conclusions

A study of the dehydrogenation thermodynamic properties of $Ti_{16}V_{60}Cr_{24-x}Fe_x$ ($x = 0, 4, 8, 12, 16, 20, 24$) alloys allowed us to draw the following conclusions: first of all, the plateau pressure and the desorbed hydrogen capacity decreased with an increasing Fe proportion. Enthalpy and entropy both diminished when increasing the amount of Fe. Moreover, ΔS , as function of the ΔH plot, showed a linear variation that indicates the possible existence of EEC with $T_{comp} = 254$ K. Finally, the values of (K, CQF) derived from ΔS and ΔH are outside the 99% confidence contour. This means that the origin of the EEC is not a statistical effect at the 99% confidence level.

Author Contributions: All experiments were performed by F.R. under the supervision of J.H. J.H. and F.R. analyzed the results and wrote the paper. All authors have read and agreed to the published version of the manuscript.

Funding: This research received no external funding.

Data Availability Statement: All data and materials are available on request from the corresponding author. The data are not publicly available due to ongoing researches using a part of the data.

Acknowledgments: The authors would like to thank Ronald Griessen of VU University, Amsterdam, for useful discussion.

Conflicts of Interest: The authors declare no conflicts of interest.

References

1. Tamura, T.; Kamegawa, A.; Takamura, H.; Okada, M. Hydrogen Isotope Effects on Absorption Properties of Ti-Cr-V Alloys. *Mater. Trans.* **2003**, *44*, 641–644. [\[CrossRef\]](#)
2. Tamura, T.; Tominaga, Y.; Matsumoto, K.; Fuda, T.; Kuriwa, T.; Kamegawa, A.; Takamura, H.; Okada, M. Protium Absorption Properties of Ti-V-Cr-Mn Alloys with a b.c.c. Structure. *J. Alloys Compd.* **2002**, *330–332*, 522–525. [\[CrossRef\]](#)
3. Fuda, T.; Matsumoto, K.; Tominaga, Y.; Tamura, T.; Kuriwa, T.; Kamegawa, A.; Okada, M. Effects of Additions of BCC Former Elements on Protium Absorbing Properties of Cr-Ti-V Alloys. *Mater. Trans. JIM* **2000**, *41*, 577–580. [\[CrossRef\]](#)
4. Tsukahara, M.; Takahashi, K.; Mishima, T.; Isomura, A.; Sakai, T. Heat-Treatment Effects of V-Based Solid Solution Alloy with TiNi-Based Network Structure on Hydrogen Storage and Electrode Properties. *J. Alloys Compd.* **1996**, *243*, 133–138. [\[CrossRef\]](#)
5. Itoh, H.; Arashima, H.; Kubo, K.; Kabutomori, T.; Ohnishi, K. Improvement of Cyclic Durability of BCC s Tructured Ti-Cr-V Alloys. *J. Alloys Compd.* **2005**, *404–406*, 417–420. [\[CrossRef\]](#)
6. Lototsky, M.V.; Yartys, V.A.; Zavalii, I.Y. Vanadium-Based BCC Alloys: Phase-Structural Characteristics and Hydrogen Sorption Properties. *J. Alloys Compd.* **2005**, *404–406*, 421–426. [\[CrossRef\]](#)
7. Reilly, J.J.; Wiswall, R.H. The Higher Hydrides of Vanadium and Niobium. *Inorg. Chem.* **1970**, *9*, 1678–1682. [\[CrossRef\]](#)
8. Seo, C.Y.; Kim, J.H.; Lee, P.S.; Lee, J.Y. Hydrogen Storage Properties of Vanadium-Based b.c.c. Solid Solution Metal Hydrides. *J. Alloys Compd.* **2003**, *348*, 252–257. [\[CrossRef\]](#)
9. Kamble, A. Effect of Additives, Heat Treatment and Mechanical Deformations on Hydrogen Storage Properties of BCC Alloys. Ph.D. Thesis, Université du Québec à Trois, Rivières, QC, Canada, 2018.
10. Sleiman, S.; Huot, J. Microstructure and First Hydrogenation Properties of TiHfZrNb1-XV1 + x Alloy for x = 0, 0.1, 0.2, 0.4, 0.6 and 1. *Molecules* **2022**, *27*, 1054. [\[CrossRef\]](#)
11. Kamble, A.; Huot, J.; Sharma, P. Effect of Addition of Zr, Ni, and Zr-Ni Alloy on the Hydrogen Absorption of Body Centred Cubic 52Ti-12V-36Cr Alloy. *Int. J. Hydrogen Energy* **2018**, *43*, 7424–7429. [\[CrossRef\]](#)
12. Ravalison, F.; Rabkin, E.; Huot, J. Methods to Improve the First Hydrogenation of the Vanadium-Rich BCC Alloy Ti 16 V 60 Cr 24. *Hydrogen* **2022**, *3*, 303–311. [\[CrossRef\]](#)
13. Dixit, V.; Huot, J. Investigation of the Microstructure, Crystal Structure and Hydrogenation Kinetics of Ti-V-Cr Alloy with Zr Addition. *J. Alloys Compd.* **2019**, *785*, 1115–1120. [\[CrossRef\]](#)
14. Khajavi, S.; Rajabi, M.; Huot, J. Effect of Cold Rolling and Ball Milling on First Hydrogenation of Ti0.5Zr0.5 (Mn1-XFex) Cr1, X = 0, 0.2, 0.4. *J. Alloys Compd.* **2019**, *775*, 912–920. [\[CrossRef\]](#)
15. Sleiman, S.; Aliouat, A.; Huot, J. Materials Enhancement of First Hydrogenation of Ti 1 V 0.9 Cr 1.1 BCC Alloy by Cold Rolling and Ball Milling. *Materials* **2020**, *13*, 3106. [\[CrossRef\]](#) [\[PubMed\]](#)
16. Liu, S.; Cui, C.; Wang, X.; Li, N.; Shi, J.; Cui, S.; Chen, P. Effect of Cooling Rate on Microstructure and Grain Refining Behavior of in Situ CeB6/Al Composite Inoculant in Aluminum. *Metals* **2017**, *7*, 204. [\[CrossRef\]](#)
17. Lang, J.; Huot, J. A New Approach to the Processing of Metal Hydrides. *J. Alloys Compd.* **2011**, *509*, L18–L22. [\[CrossRef\]](#)
18. Kumar, S.; Jain, A.; Ichikawa, T.; Kojima, Y.; Dey, G.K. Development of Vanadium Based Hydrogen Storage Material: A Review. *Renew. Sustain. Energy Rev.* **2017**, *72*, 791–800. [\[CrossRef\]](#)
19. Strozi, R.B.; Silva, B.H.; Leiva, D.R.; Zlotea, C.; Botta, W.J.; Zepon, G. Tuning the Hydrogen Storage Properties of Ti-V-Nb-Cr Alloys by Controlling the Cr/(TiVNb) Ratio. *J. Alloys Compd.* **2023**, *932*, 167609. [\[CrossRef\]](#)
20. Yukawa, H.; Teshima, A.; Yamashita, D.; Ito, S.; Morinaga, M.; Yamaguchi, S. Alloying Effects on the Hydriding Properties of Vanadium at Low Hydrogen Pressures. *J. Alloys Compd.* **2002**, *337*, 264–268. [\[CrossRef\]](#)
21. Verbetsky, V.N.; Zotov, T.A.; Tatarintsev, A.V.; Movlaev, E.A. Hydrogen Sorption Properties of V1-x Crx (x = 0.1–0.5) Alloys. *Inorg. Mater.* **2013**, *49*, 149–152. [\[CrossRef\]](#)
22. Kazumi, T.; Tamura, T.; Kamegawa, A.; Takamura, H.; Okada, M. Effect of Absorption-Desorption Cycles on Structure and Stability of Protides in Ti-Cr-V Alloys. *Mater. Trans.* **2002**, *43*, 2748–2752. [\[CrossRef\]](#)
23. Asano, K.; Hayashi, S.; Nakamura, Y. Enhancement of Hydrogen Diffusion in the Body-Centered Tetragonal Monohydride Phase of the V-H System by Substitutional Al Studied by Proton Nuclear Magnetic Resonance. *Acta Mater.* **2015**, *83*, 479–487. [\[CrossRef\]](#)
24. Kagawa, A.; Ono, E.; Kusakabe, T.; Sakamoto, Y. Absorption of Hydrogen by Vanadium-Rich VTi-Based Alloys. *J. Less-Common Met.* **1991**, *172–174*, 64–70. [\[CrossRef\]](#)
25. Lynch, J.F.; Reilly, J.J.; Millot, F. The Absorption of Hydrogen by Binary Vanadium-Chromium Alloys. *J. Phys. Chem. Solids* **1978**, *39*, 883–890. [\[CrossRef\]](#)
26. Wang, J.Y.; Jeng, R.R.; Nieh, J.K.; Lee, S.; Lee, S.L.; Bor, H.Y. Comparing the Hydrogen Storage Alloys-TiCrV and Vanadium-Rich TiCrMnV. *Int. J. Hydrogen Energy* **2007**, *32*, 3959–3964. [\[CrossRef\]](#)
27. Tsukahara, M. Hydrogenation Properties of Vanadium-Based Alloys with Large Hydrogen Storage Capacity. *Mater. Trans.* **2011**, *52*, 68–72. [\[CrossRef\]](#)
28. Yan, Y.; Li, Z.; Wu, Y.; Zhou, S. Hydrogen Absorption-Desorption Characteristic of (Ti0.85Zr0.15)1.1Cr1-XMoxMn Based Alloys with C14 Laves Phase. *Prog. Nat. Sci. Mater. Int.* **2022**, *32*, 143–149. [\[CrossRef\]](#)
29. Kumar, A.; Muthukumar, P.; Kumar, E.A. Absorption Based Solid State Hydrogen Storage System: A Review. *Sustain. Energy Technol. Assess.* **2022**, *52*, 102204. [\[CrossRef\]](#)
30. Aoki, M.; Noritake, T.; Ito, A.; Ishikiriyama, M.; Towata, S.I. Improvement of Cyclic Durability of Ti-Cr-V Alloy by Fe Substitution. *Int. J. Hydrogen Energy* **2011**, *36*, 12329–12332. [\[CrossRef\]](#)

31. Towata, S.I.; Noritake, T.; Itoh, A.; Aoki, M.; Miwa, K. Effect of Partial Niobium and Iron Substitution on Short-Term Cycle Durability of Hydrogen Storage Ti-Cr-V Alloys. *Int. J. Hydrogen Energy* **2013**, *38*, 3024–3029. [[CrossRef](#)]
32. Shashikala, K.; Banerjee, S.; Kumar, A.; Pai, M.R.; Pillai, C.G.S. Improvement of Hydrogen Storage Properties of TiCrV Alloy by Zr Substitution for Ti. *Int. J. Hydrogen Energy* **2009**, *34*, 6684–6689. [[CrossRef](#)]
33. C. Julien, J.P.; Pereira-Ramos, A.M. (Eds.) *New Trends in Intercalation Compounds for Energy Storage NATO Science Series*; Kluwer Academic Publishers: Dordrecht, The Netherlands, 2003; ISBN 9781402005954.
34. Kohlmann, H. Metal Hydrides. *Encycl. Phys. Sci. Technol.* **2003**, 441–458. [[CrossRef](#)]
35. Schwarz, J.A.; Felton, L.E. Compensating Effects in Electromigration Kinetics. *Solid State Electron.* **1985**, *28*, 669–675. [[CrossRef](#)]
36. Widenhorn, R.; Mündermann, L.; Rest, A.; Bodegom, E. Meyer-Neldel Rule for Dark Current in Charge-Coupled Devices. *J. Appl. Phys.* **2001**, *89*, 8179–8182. [[CrossRef](#)]
37. Ullah, M.; Singh, T.B.; Sitter, H.; Sariciftci, N.S. Meyer-Neldel Rule in Fullerene Field-Effect Transistors. *Appl. Phys. A Mater. Sci. Process.* **2009**, *97*, 521–526. [[CrossRef](#)]
38. Andreasen, A.; Vegge, T.; Pedersen, A.S. Compensation Effect in the Hydrogenation/Dehydrogenation Kinetics of Metal Hydrides. *J. Phys. Chem. B* **2005**, *109*, 3340–3344. [[CrossRef](#)]
39. Griessen, R.; Boelsma, C.; Schreuders, H.; Broedersz, C.P.; Gremaud, R.; Dam, B. Single Quality Factor for Enthalpy-Entropy Compensation, Isoequilibrium and Isokinetic Relationships. *ChemPhysChem* **2020**, *21*, 1632–1643. [[CrossRef](#)]
40. Cornish-Bowden, A. Enthalpy-Entropy Compensation: A Phantom Phenomenon. *J. Biosci.* **2002**, *27*, 121–126. [[CrossRef](#)]
41. Patelli, N.; Calizzi, M.; Pasquini, L. Inorganics Interface Enthalpy-Entropy Competition in Nanoscale Metal Hydrides. *Inorganics* **2018**, *6*, 13. [[CrossRef](#)]
42. Perez-Benito, J.F.; Mulero-Raichs, M. Enthalpy-Entropy Compensation Effect in Chemical Kinetics and Experimental Errors: A Numerical Simulation Approach. *J. Phys. Chem. A* **2016**, *120*, 7598–7609. [[CrossRef](#)]
43. Griessen, R.; Dam, B. Simple Accurate Verification of Enthalpy-Entropy Compensation and Isoequilibrium Relationship. *ChemPhysChem* **2021**, *22*, 1774–1784. [[CrossRef](#)] [[PubMed](#)]
44. Francia, R.; Huot, J. Microstructure and First Hydrogenation Properties of Ti₁₆V₆₀Cr₂₄–xFe_x + 4 Wt.% Zr Alloy for x = 0, 4, 8, 12, 16, 20, 24. *Energies* **2023**, *16*, 5360. [[CrossRef](#)]
45. Akiba, E.; Okada, M. Metallic Hydrides III: Cubic Solid- Solution Alloys. *MRS Bull.* **2002**, *27*, 699–703. [[CrossRef](#)]
46. Lynch, J.F.; Maeland, A.J.; Libowitz, G.G. Lattice Parameter Variation and Thermodynamics of Dihydride Formation in the Vanadium-Rich V–Ti–Fe/H₂ System*. *Z. FÜR Phys. Chem.* **1985**, *145*, 51–59. [[CrossRef](#)]

Disclaimer/Publisher’s Note: The statements, opinions and data contained in all publications are solely those of the individual author(s) and contributor(s) and not of MDPI and/or the editor(s). MDPI and/or the editor(s) disclaim responsibility for any injury to people or property resulting from any ideas, methods, instructions or products referred to in the content.